Eur. Phys. J. Special Topics **227**, 2025–2035 (2019)

https://doi.org/10.1140/epjst/e2018-800050-3

THE EUROPEAN PHYSICAL JOURNAL SPECIAL TOPICS

Regular Article

# Spatial coupling of quantum-anomalous-Hall and chiral-Majorana modes

Javier Osca[1], Marc Alomar[1], and Llorenç Serra[1,2,a]

[1] Institute for Cross-Disciplinary Physics and Complex Systems IFISC (CSIC-UIB), 07122 Palma, Spain
[2] Physics Department, University of the Balearic Islands, 07122 Palma, Spain

Received 12 April 2018 / Received in final form 26 June 2018
Published online 18 January 2019

**Abstract.** We calculate density and current spatial distributions of a 2D model junction between a normal QAH contact and a superconducting QAH region hosting propagating (chiral) Majorana modes. We use a simplified Hamiltonian describing the spatial coupling of the modes on each side of the junction, as well as the related junction conductance. We study how this coupling is affected by orbital effects caused by an external magnetic field.

## 1 Introduction

Majorana states in Condensed Matter have been a hot topic for a few years now [1–11]. Different experiments have been carried out in order to demonstrate the actual existence of such topological states. Majorana modes are characterized by being chargeless and spinless edge states, hence most of the experiments aiming at their detection are based on identifying characteristic signatures on the electrical conductance of devices attached to them [12–16]. To obtain Majorana states one needs the presence of superconductivity, therefore the typical scenario usually requires a contact between a normal lead and a hybrid proximity-coupled semiconductor-superconductor. As topological states, Majorana modes are separated by an energy gap that protects them from other normal states and local sources of noise, a robustness that might allow the use of such states for topological quantum computing.

In many ways Majoranas can be understood as non-local split Fermions. In this sense there are two kinds of Majorana states: non-propagating Majorana states appearing at the ends of (quasi) 1D nanowires and propagating chiral Majorana states formed along the edges of 2D-like hybrid structures. In this work, we will focus on the second kind. We refer, more specifically, to devices similar to those of references [16–22] consisting of a quantum Hall (QH) or quantum anomalous Hall (QAH) insulator proximity coupled with a superconductor (QAH + S). In particular, we will consider a simple model of QAH + S that does not need the presence of external magnetic fields. In this kind of systems, chiral Majorana modes propagate along the edges in a clockwise or anticlockwise manner (depending on device parameters) for finite systems.

[a] e-mail: llorens.serra@uib.es

An open infinite nanowire like the one depicted in the inset of Figure 1 may hold two pairs of counterpropagating Majorana channels, one pair at each edge of the device. In general, it has been reported that each chiral Majorana channel contributes $0.5e^2/h$ to the linear conductance of a device. However, in this work we will show that for the infinite nanowire with only one normal contact the conductance remains $e^2/h$ independently of the number of active Majorana modes (one or two), even with a finite transmission probability to the Majorana channel of $\approx 0.5$. The reason for this is that we consider a single normal contact connected to a semi-infinite Majorana device, instead of the two usual contacts in a normal-superconductor-normal arrangement. When only one normal contact (left) is present, only half of the possible Majorana channels are active, the outgoing ones. Ingoing Majorana modes into the junction would necessarily require a second (right) normal contact and therefore they are not contributing in our arrangement.

We use a method based on the evaluation of the (complex) wave numbers allowed on each side of the junction and giving the detailed spatial distribution patterns of density and currents. In addition, we study how the spatial distribution of the Majorana modes is affected by magnetic orbital effects, on top of the already present QAH physics. We show how the spatial coupling between Majorana and non-Majorana states at both sides of the junction modifies the transmission and reflection processes, and thus also the conductance. This article is divided in five parts. Sections 2 and 3 present the model and the method of resolution to determine ingoing and outgoing modes of the junction. Next, in Sections 4 and 5 we present the results without and with orbital effects of the magnetic field, respectively. Finally, a summary and outlook of the work is given in Section 6.

## 2 Model

Our main objective is to study the distribution of currents and the conductance present in a N-(QAH+S) junction where chiral Majoranas may be present. We start using a simplified model of QAH+S Hamiltonian similar to the one devised in references [17,18],

$$h_{BdG}(\mathbf{p}) = m(\mathbf{p})\sigma_z - \frac{\alpha}{\hbar}\left(p_x\sigma_y - p_y\sigma_x\right)\tau_z + \Delta(x)\,\tau_+ + \Delta(x)^*\,\tau_- \,, \tag{1}$$

where $m(\mathbf{p}) = m_0 + m_1\mathbf{p}^2$, with $m_0$ and $m_1$ known material parameters. As usual, the $\sigma$'s and $\tau$'s represent Pauli matrices for spin and isospin, respectively. We will consider $\alpha$ a known parameter related with the quasi-particle mass governing the shape of the Dirac cone for energies near its apex. In this work, we set $\alpha \equiv 1$ as our unit for practical reasons. We will assume superconductivity achieved by proximity coupling between the QAH semiconductor and a metallic superconductor. The union between a superconducting and non superconducting region will be achieved through the spatial variation of the superconductor coupling constant $\Delta(x)$.

The numerical results of this work will be presented in natural units of the problem, i.e., taking $2m_1$, $\hbar$ and $\alpha$ as unit values. That is, our length and energy units are $L_U \equiv L_{so} = 2m_1\hbar^2/\alpha$ and $E_U = \alpha^2/2m_1\hbar^2$. The physical values for $L_U$ and $E_U$ are determined once $m_1$ and $\alpha$ are known for a specific system. For definiteness, assuming $(2m_1)^{-1} \approx 0.06\,m_e$ [23], where $m_e$ is the bare electron mass, and $\alpha \approx 0.2$ eVÅ it is $E_U = 0.5\,\text{meV}$ and $L_U = 50\,\text{nm}$.

This model provides two phase boundaries with a critical value of the $m_0$ parameter, $m_0^{(c)} = \pm|\Delta|$. For large positive values of $m_0$ the device will be in a trivial phase while for large negative ones a phase of Chern number $\mathcal{C} = 2$ will arise with two

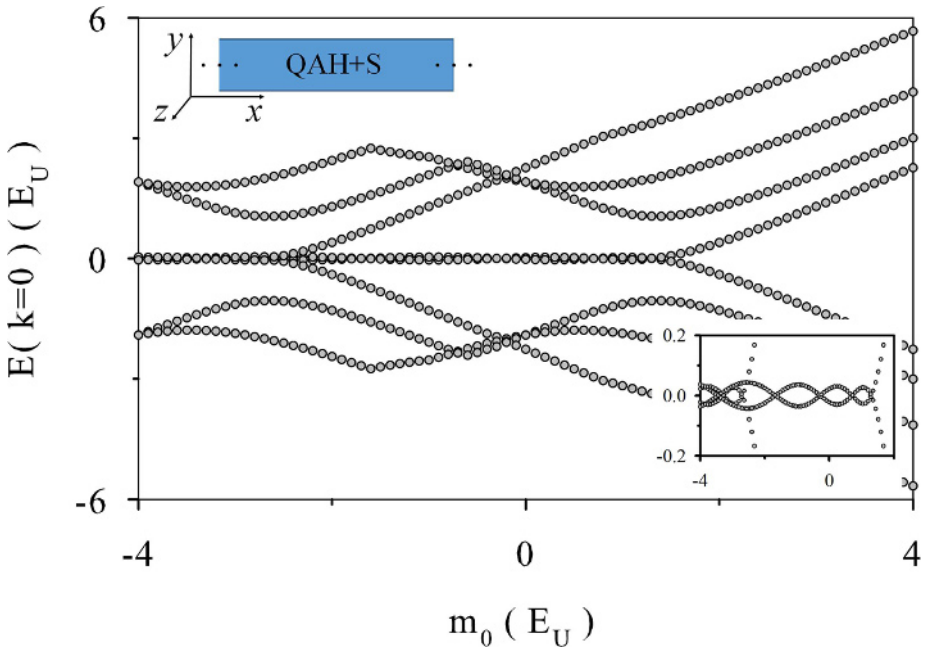


**Fig. 1.** $E(k = 0)$ as a function of the material parameter $m_0$ for a QAH thin slab of $L_y = 5L_U$ proximity coupled with a superconductor yielding strength $\Delta = 2E_U$. A sketch of the infinite system used for this band structure calculation is given in the upper inset. Notice the phase transitions at $m_0 \approx \pm\Delta$, as indicated by the presence of zero modes. The remaining small oscillation around zero energy, zoomed in in the lower inset, is a finite size effect.

chiral Majoranas attached to each edge of the device. For intermediate values of $m_0$, between the two phase boundaries, there is a single Majorana phase of Chern number one (see Fig. 1). The phase-transition boundaries may differ slightly from these values due to the transversal confinement, in a similar manner as in non-chiral Majorana nanowires [24]. Of course, the effect of the transversal confinement becomes negligible in wide enough wires.

The presence of the Majorana modes is signaled by a pair of topological bands at wavenumber $k = 0$ for the translationally invariant (infinite) wire. In Figure 1, this can be seen with a plot of the energy $E(k = 0)$ as a function of $m_0$. The presence of zero-energy modes indicate the Majorana phases, in good agreement with the expected critical values. The bulk-edge correspondence principle ensures that the critical value $m_0^{(c)}$ also indicates when chiral Majoranas will appear in a semi-infinite nanowire or in the superconducting region of the N-(QAH+S) junction studied in this work.

## 3 Method

We want to calculate the distribution of currents for a junction between a normal QAH material and a material of the same kind proximity coupled with a superconductor (see Fig. 2 for a graphical representation of the device). The numerical method was already used by us to calculate local currents and conductance in N-S junctions for non-chiral Majoranas in references [25,26], with some technical differences as briefly explained below.

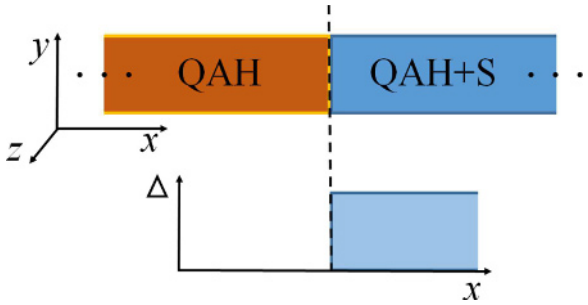


**Fig. 2.** Graphical description of the nanowire junction considered in this work, an infinite QAH thin slab with half of the slab proximity coupled with a superconductor. The junction interface separates normal and superconducting regions. On the left side there is a normal QAH region while on the right side there is a hybrid QAH+superconducting region with a non-zero $\Delta$.

The overall idea is that of a matching method for two different sets of asymptotic solutions, for a given energy $E$, one for each side of the junction and characterized by a $k$ wave number, $\Psi_k(x, y, \eta_\sigma, \eta_\tau) = \phi_k(y, \eta_\sigma, \eta_\tau)e^{ikx}$. These asymptotic solutions for the left and right contacts are assumed to be known for a large-enough set of wave numbers, with $k$ being either real (propagating) or complex (evanescent) [27]. Typically, we find well converged results with a total of $\approx 200$ $k$-modes. The full solution for the left and right sides of the junction ($c = L, R$) is given by a superposition of the corresponding set of modes,

$$\Psi^{(c)}(x, y, \eta_\sigma, \eta_\tau) = \sum_k d_k^{(c)}\, e^{ikx}\, \phi_k(y, \eta_\sigma, \eta_\tau)\,. \tag{2}$$

The wavenumbers and the transverse eigenstates can be obtained numerically as solutions of the BdG Hamiltonian for each contact, where $\sum_{\eta_\sigma \eta_\tau} \int dy\, |\phi_k|^2 = 1$. The coefficients $d_k^{(c)}$ that determine the strength of each channel are obtained from the matching algorithm [25,26].

The distribution of currents is calculated from the wave functions given by equation (2). We consider three different kinds of densites $\rho_a(x, y)$ and currents $\mathbf{j}_a(x, y)$, where subindex $a$ may be $a = qp, c, s$ for quasiparticle, charge, and spin, respectively. Quasi-particle distributions are given by

$$\rho_{qp}(x, y) = \Psi^*(x, y)\Psi(x, y), \tag{3}$$
$$\mathbf{j}_{qp}(x, y) = \mathrm{Re}\,[\,\Psi^*(x, y)\,\hat{\mathbf{v}}_{qp}\,\Psi(x, y)\,]\,, \tag{4}$$

where the velocities are given by $\hat{v}_{qp,x} = \partial\mathcal{H}/\partial p_x$ and $\hat{v}_{qp,y} = \partial\mathcal{H}/\partial p_y$. Quasiparticle density and current fulfill a continuity equation $\partial\rho_{qp}(x, y)/\partial t = \nabla \cdot \mathbf{j}_{qp}(x, y)$ because the model has no sources or sinks of quasiparticles. With the Hamiltonian of equation (1) it is,

$$\hat{v}_{qp,x} = -i\hbar 2m_1\partial_x\sigma_z - \frac{\alpha}{\hbar}\sigma_y\tau_z\,, \tag{5}$$
$$\hat{v}_{qp,y} = -i\hbar 2m_1\partial_y\sigma_z + \frac{\alpha}{\hbar}\sigma_x\tau_z\,. \tag{6}$$

Substitution of equations (5) and (6) in equation (4) lead to the more familiar expressions

$$\mathbf{j}_{qp}(x,y) = 2\hbar m_1 \mathrm{Im}\left[\,\Psi^*(x,y)\,\nabla\sigma_z\,\Psi(x,y)\,\right] + \mathbf{j}_{so}(x,y), \tag{7}$$

where

$$\mathbf{j}_{so}(x,y) = -\frac{\alpha}{\hbar}\,\mathrm{Re}\left[\,\Psi^*(x,y)\,(\sigma_y\hat{x} - \sigma_x\hat{y})\tau_z\,\Psi(x,y)\,\right]. \tag{8}$$

The charge and spin densities are obtained by adding $-e\tau_z$ and $\sigma_z$ operators, respectively, in equation (3),

$$\rho_c(x,y) = -e\,\Psi^*(x,y)\tau_z\Psi(x,y)\;, \tag{9}$$
$$\rho_s(x,y) = \Psi^*(x,y)\sigma_z\Psi(x,y)\;. \tag{10}$$

Analogous substitutions in equation (4) yield the definitions of $\mathbf{j}_c(x,y)$ and $\mathbf{j}_s(x,y)$, the charge and spin currents.

The conductance of the junction is evaluated on the normal side as

$$g(E) = \frac{e^2}{h}\left[\,N(E) - P_{ee}(E) + P_{eh}(E)\,\right]\;, \tag{11}$$

where

$$P_{ee}(E) = \sum_{k,\eta_\sigma} d_k^{(L)}(E) \int dy \left|\phi_k^{(L)}(y,\eta_\sigma,\Uparrow)\right|^2\;, \tag{12}$$

$$P_{eh}(E) = \sum_{k,\eta_\sigma} d_k^{(L)}(E) \int dy \left|\phi_k^{(L)}(y,\eta_\sigma,\Downarrow)\right|^2\;, \tag{13}$$

are, respectively, the electron-electron ($ee$) and electron-hole ($eh$ or Andreev) reflection probabilities. As well known, normal $ee$ reflection reduces the conductance while Andreev $eh$ one increases it. Notice also that in the $k$-sums of equations (12) and (13) only propagating output modes have to be included. The coefficients $d_k^{(c)}$ for both evanescent and propagating modes are obtained from the numerical algorithm, with the exception of the input channels that are set to one for normalization purposes. We consider as input channels the electron propagating solutions in the normal lead with a quasi-particle flow into the junction. As a peculiarity of this problem, we found that for $E = 0$ and $k = 0$ some instabilities in the flow calculation are obtained. They are due to state degeneracies not allowing the algorithm to properly identify the channels. They are simply resolved, however, by using a nonzero (small) value for $E$.

## 4 Current distributions

In Figure 3 we display the quasi-particle current distribution (arrows) overprinted on their corresponding quasiparticle densities (color or gray-shaded) for two different scenarios. Figures 3a and 3c are for the case when the right side of the junction has a Chern number one, i.e., with a pair of topological bands crossing zero energy. Therefore, for energies below the gap there is a propagating Majorana mode attached to a system edge. On the other hand, Figures 3b and 3d correspond to the case of Chern number two, with an additional pair of bands crossing zero energy. In this

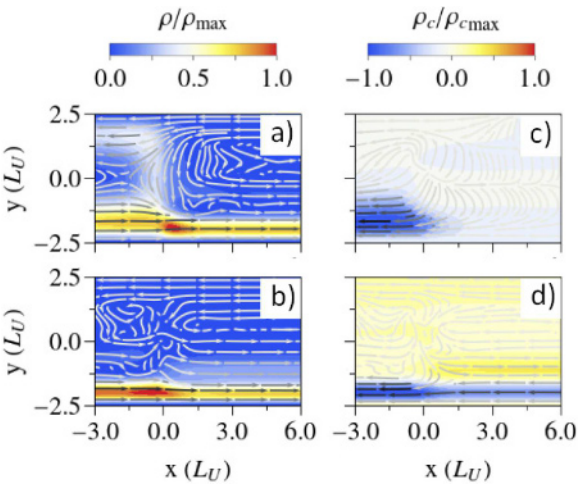


**Fig. 3.** Quasi-particle current overprinted on its corresponding probability density for a NS junction with (a) one chiral Majorana mode in the superconducting side of the junction (that is, $\mathcal{C} = 1$ topological phase); (b) two simultaneous Chiral Majorana modes in the superconducting region ($\mathcal{C} = 2$ topological phase). (c) and (d) the charge current and densities corresponsing to the cases in (a) and (b), respectively. The material parameter for (a) is $m_0 = -1E_U$ while for (b) is $m_0 = -3E_U$. The rest of the parameters are $L_y = 5\,L_U$, $\Delta = 2.0E_U$ and $E = 0.1E_U$. Note that we take $\alpha = 1E_U L_U$ and $m_1 = 0.5E_U L_U^2/\hbar^2$.

latter case we have simultaneously two propagating Majorana modes attached to the same edge. The first thing we notice is that only the lower edge shows an attached Majorana channel on the right side of the junction. The reason behind this difference between upper and lower edges is that in an infinite NS junction there are no counter propagating modes. That is, the Majorana channel in the lower border is an outgoing channel. An ingoing Majorana channel would appear on the upper edge in case we considered a second junction with a normal lead on the right of the superconductor region, with its corresponding incident modes.

As seen in Figures 3a and 3c, with only one pair of topological bands in the superconductor region ($\mathcal{C} = 1$) an incident electron channel from the normal region will be transmitted to a Majorana channel in the superconducting region. Note that the Majorana channel is associated with a zero charge density and zero charge current. The transmission probability is $P_T = 0.5$ and, nevertheless, the conductance $g(E)$ is still one quantum $g(E) = e^2/h$. The reason behind this apparent paradox is the distribution of probability between the reflected $ee$ and $eh$ channels. The electronic incident channel is partially reflected back in equal measure as an electron and as a hole through Andreev reflection, $P_{ee} = 0.25$ and $P_{eh} = 0.25$. This is not in contradiction with current literature finding a conductance of $g(E) = 0.5e^2/h$ due to the Majorana mode because, as explained above, we are considering a NS junction with a single normal lead and therefore neglecting the effect in the junction from Majorana counterpropagating states with an origin in a second lead. As a matter of fact an NSN double junction can be seen in a simple way as a series combination of two NS single junctions and therefore a reduction of $\approx 2$ in conductance is to be expected in the double junction. In this sense, the NS reflected channels have several peculiarities. First, their charge current and densities add up to zero and the same happens with their spin current and density (see Fig. 4). The incident electron channel is responsible for an ingoing spin current into the Majorana mode, signaling the topological state of the superconductor.

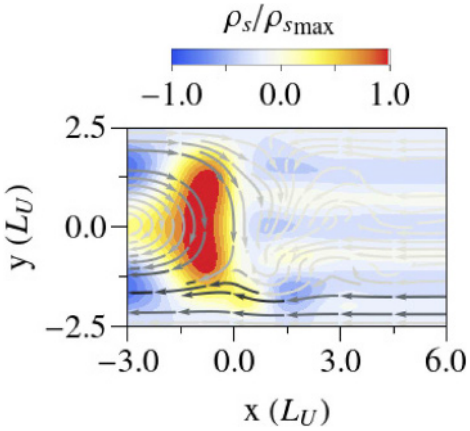


**Fig. 4.** Spin current overprinted on the spin density for the case when the superconductor holds a single chiral Majorana mode. The Hamiltonian parameters are $L_y = 5\,L_U$, $m_0 = -1E_U$, $\Delta = 2E_U$ and $E = 0.1E_U$.

On the other hand, in Figures 3b and 3d we can see the case with two pairs of topological bands active on the right side of the junction. In this case the incident electronic channel just goes through the junction without reflection. That is not surprising because two chiral Majorana channels add up to a single electron channel. We can see in Figure 3d how charge neutrality of the chiral Majoranas on the right side has been lost with the presence of charge current in the lower superconducting border. Furthermore, the available edge channels degrade with increasing energy of the incident channel (i.e., the quality of the edge modes is worse as we deviate more and more from zero energy and approach the gap energy). For this reason we use a small value $E = 0.1E_U$. This charge current is thus a manifestation of the Fermionization of the two Majoranas in the $\mathcal{C} = 2$ phase. With narrower slabs similar charge current may build up even in the $\mathcal{C} = 1$ topological phase due to finite size effects for smaller $L_y$'s. However, this is already not the case in Figure 3c with $L_y = 5\,L_U$.

In Figure 5 we can see the case when the superconductor is in a trivial state. In previous figures we considered an homogeneous infinite semiconductor thin slab with a junction separating the proximity coupled superconducting region from the non-superconducting one. However, here for pedagogical reason we consider that the junction separates two semiconductors having different material parameter $m_0$. The reason is that no open incident channels are available in the normal region for the range of values where the superconducting region is in a trivial phase. Therefore, we maintain the left side of the junction at a value of $m_0$ that allows for an electronic incident channel. The result is a perfect electron-electron reflection of the quasi-particle current. Therefore the overall charge and spin current in the contact remains zero.

## 5 Orbital effects

Until now we have considered the behavior of the junction mainly regarding variations of the material parameter $m_0$. In the underlying physical model, this parameter relates to the magnetization of the material. In this section, we want to explore how the inclusion of orbital effects due to an external magnetic field may affect the results of our model. The strength of magnetic orbital effects is set by the magnetic length $l_z$, defined as $l_z^2 = \hbar c/eB$. We consider a fully perpendicular magnetic field to the

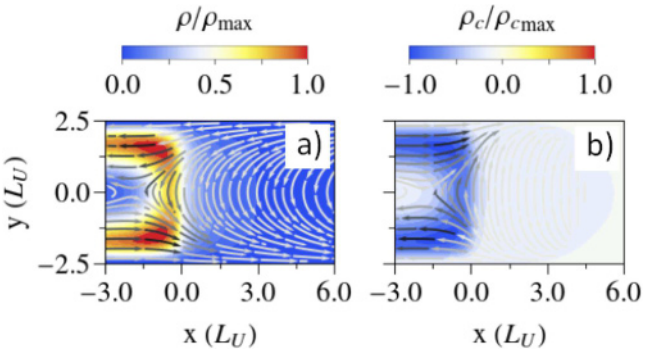


**Fig. 5.** (a) Quasi-particle current overprinted on the probability density for the case when the superconducting side of the junction is in a trivial phase. (b) The same of (a) for the charge current and density. In order to have open channels available to probe the superconductor, the material parameter $m_0$ takes different values on the left and right sides; it is $m_0 = -1E_U$ on the left and $m_0 = 2E_U$ on the right. The rest of the parameters are the same of preceding figures.

sample using a Landau gauge centered on $y = 0$ through the magnetic substitution $p_x \to p_x - \hbar y/l_z^2$. We also add the required Pauli matrix $\tau_z$ to properly consider the electron-hole symmetry of the problem [24].

The physical scenario of the model is a rather strong intrinsic magnetization term ($m_0$) and weaker magnetic orbital terms ($l_z$). The actual strength of the magnetic field is proportional to $l_z^{-2}$. With our length unit $L_U = 50\,\text{nm}$ the field in teslas is given by $B/\text{T} \approx 0.26\,(l_z/L_U)^{-2}$, i.e., 1 T is roughly corresponding to $l_z^{-2} = 4L_U^{-2}$. Of course, it is important that $B$ does not exceed the critical field of the superconductor needed for the proximity effect, which is also $\approx 1$T for a superconducting thin Nb film [20].

The effects of electronic orbital motion on the QAH thin slab are twofold. First, if the external magnetic field is too large the edge channels disappear. This is not surprising because many chiral Majorana devices are quantum Hall devices with the addition of superconductivity. This way, different strengths of the field may enable or disable the edge propagating channels. In a certain way we are including here a competition between the QH and QAH effects. We can see in Figure 6a the conductance, and the different probabilities of transmission and reflection for a QAH normal-superconductor junction as a function of the magnetic length. At a certain value of the magnetic length ($l_z^{-2} \approx 1.3L_U^{-2}$) the QAH propagating channels are closed on the normal side of the junction and only evanescent modes remain.

On the other hand, the second effect of the orbital motion is to effectively change the width of the nanowire due to magnetic confinement when $l_z < L_y$ (with $L_y$ the transverse width). This way, the distance of the QAH and chiral Majoranas with respect to the device edges increases, as can be seen comparing Figure 6b with Figure 3a. However, the most interesting feature is the separation of the propagating states from their respective edges and how this changes differently on each side of the junction for increasing external field. This affects how the electronic incident channel couples with the outgoing chiral Majorana mode on the superconductor side. Therefore, the transmission and reflection probabilities (and thus the conductance) are modified by the relative position of the channels caused by the presence of the orbital motion.

The oscillations in reflection and transmission probabilities, and thus in conductance, are due to changes in the transversal positions of the topological states.

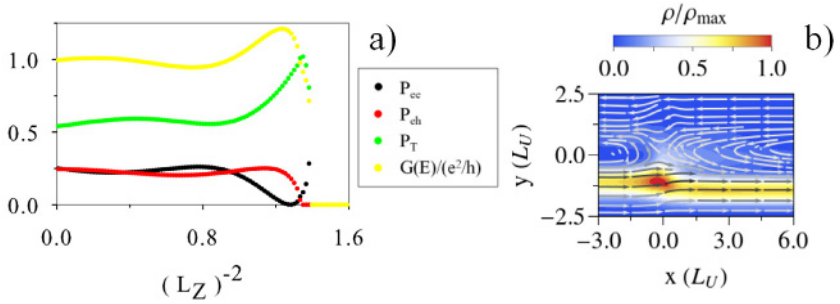


**Fig. 6.** (a) Probabilities of reflection $P_{ee}$, Andreev reflection $P_{eh}$, transmission $P_T$ and conductance $g(E)$ of an incident electronic channel in a QAH slab with a normal-superconductor junction. The probabilities and conductance are shown as a function of the inverse squared magnetic length $l_z^{-2}$ that is directly proportional to the field. At zero field the device holds a chiral Majorana nanowire in the superconducting side of the junction. The Hamiltonian parameters are $m_0 = -1.0E_U$, $\Delta = 2.0E_U$ and $E = 0.1E_U$. (b) Quasi-particle current and probability density for $l_z^{-2} = 1.2L_U^{-2}$. Note that, in comparison with Figure 3a, the position of the edge states with respect to the confinement wall has changed. There are also differences between the left and right edge states relative position in the $y$ direction.

However, these changes are abruptly hindered by the disappearance of the propagating channels in the normal lead with increasing magnetic field. In the rest of the paper we will not consider orbital effects in the normal lead of the junction, assuming that we have shielded or dampened the magnetic field in that region. This way we always have a propagating channel opened in the normal contact to probe the behavior of the chiral modes under the effects of the orbital motion.

In Figure 7 we consider a QAH slab with orbital effects active only on the superconducting side. The superconducting region is tuned to hold a single Majorana channel at zero external field. We can see in Figure 7a (at the left of the vertical dashed line) how the transmission probability slightly decreases while the normal reflection increases with increasing magnetic strength. The reason is the change in spatial alignment between the incident and the Majorana channels, as shown in Figure 7b. This behavior persists up to the strength value marked as a black vertical dashed line. From that point onwards the magnetic effective confinement is too narrow to allow the nanowire to hold the transversal length of the Majorana. Therefore the propagating chiral Majorana mode disappears and only evanescent modes remain in the superconducting region. This is signaled by a zero transmission probability and the dominance of the Andreev effect as the main reflection mechanism. Electron-hole reflection probability rises to one and the conductance achieves its maximum value of two.

Finally, in Figure 8 we consider the same slab but with the superconducting region tuned to hold two Majorana channels at zero external field. In Figure 8a the first vertical dashed line signals the transition from a state with two Majorana edge states to a single Majorana state, while the second one signals the loss of both Majorana channels. The first transition is followed by a change in the transmission probability $P_T \approx 1$ to $P_T \approx 0.5$ as we expect from the loss of one of the two Majorana channels. Accordingly, the electron and hole reflection probabilities rise from zero to $P_{ee} \approx P_{eh} \approx 0.25$. Note, however, that here the change of the probabilities with the magnetic strength is not abrupt (probably because of large transverse finite size effects). The change is also smooth at the transition from one to zero active Majorana channels. This causes the conductance to oscillate while the system evolves between different conductance plateaus with smooth oscillations.

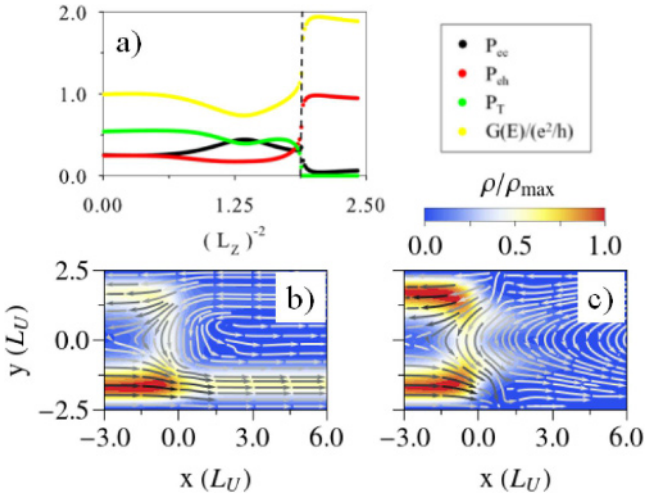


**Fig. 7.** (a) Same as in Figure 6a, but with the external magnetic field applied only to the right side of the junction. This way we avoid the channel closing on the normal side and we can probe the junction behavior for higher magnetic fields. At zero field the device holds a chiral Majorana mode in the superconducting side of the junction and the vertical dotted line signals the strength for which this Majorana mode disappears. The material parameter $m_0 = -1E_U$ is constant all along the slab, while the rest of the Hamiltonian parameters are the same as above. (b) and (c) Quasi-particle current and probability density at strengths of the external field corresponding to $l_z^{-2} = 1.2L_U^{-2}$ and $l_z^{-2} = 2.4L_U^{-2}$, respectively. Note that only evanescent modes remain on the right side in panel c).

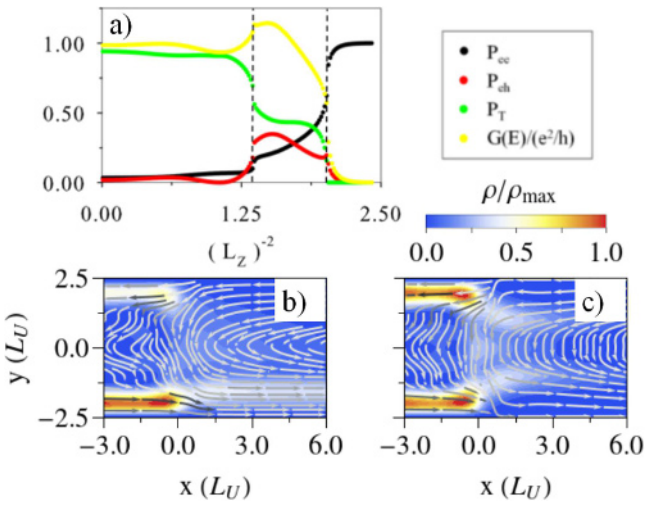


**Fig. 8.** (a) Same as in Figure 7a but with a material parameter $m_0 = -3E_U$. The rest of the Hamiltonian parameters are the same as above. This way, at zero field the device holds two chiral Majorana modes in the superconducting side of the junction. Each vertical dotted line in (a) signals the strength for which one Majorana mode is lost. (b) and (c) Quasi-particle current and probability density for strengths of the external field at the right side of the junction corresponding to $l_z^{-2} = 1.6L_U^{-2}$ and $l_z^{-2} = 2.4L_U^{-2}$, respectively.

## 6 Conclusion

We have studied how the conductance in a normal-superconductor junction with chiral Majorana modes is related to the spatial distribution of currents using a simplified model. In particular, we have shown how the spatial coupling of the propagating modes on the different sides of the junction is relevant to explain the observed results. Furthermore, we have introduced the effect of the orbital motion in the model to investigate how this coupling is affected by a magnetic field. It is the objective of future work to apply this type of analysis to a more realistic physical model, like that of reference [16], where we expect to observe similar behaviors plus some additional ones. The reason is that many of these models may be rewritten in terms of one or several coupled copies of the present one.

This work was funded by MINEICO-Spain, grant MAT2017-82639.

## References

1. C. Nayak, S.H. Simon, A. Stern et al., Rev. Mod. Phys. **80**, 1083 (2008)
2. X.-L. Qi, S.-C. Zhang, Rev. Mod. Phys. **83**, 1057 (2011)
3. J. Alicea, Y. Oreg, G. Refael et al., Nat. Phys. **7**, 412 (2011)
4. T.D. Stanescu, S. Tewari, J. Phys.: Condens. Matter **25**, 233201 (2013)
5. C.W.J. Beenakker, Ann. Rev. Condens. Matter Phys. **4**, 113 (2013)
6. M. Franz, Nat. Nanotechnol. **8**, 149 (2013)
7. S.R. Elliott, M. Franz, Rev. Mod. Phys. **87**, 137 (2015)
8. R. Aguado, Riv. Nuovo Cimento **40**, 523 (2017)
9. R.M. Lutchyn, E.P.A.M. Bakkers, L.P. Kouwenhoven et al., arXiv:1707.04899 (2017)
10. R.M. Lutchyn, J.D. Sau, S. Das Sarma, Phys. Rev. Lett. **105**, 077001 (2010)
11. Y. Oreg, G. Refael, F. von Oppen, Phys. Rev. Lett. **105**, 177002 (2010)
12. V. Mourik, K. Zuo, S.M. Frolov et al., Science **336**, 6084, 1003 (2012)
13. Ö. Gül, H. Zhang, J.D.S. Bommer et al., Nat. Nanotechnol. **13**, 192 (2018)
14. M.T. Deng, C.L. Yu, G.Y. Huang et al., Nano Lett. **12**, 6414 (2012)
15. A. Das, Y. Ronen, Y. Most et al., Nat. Phys. **8**, 887895 (2012)
16. Q.L. He, L. Pan, A.L. Stern et al., Science **357**, 294 (2017)
17. X.-L. Qi, Y.-S. Wu, S.-C. Zhang, Phys. Rev. B **74**, 085308 (2006)
18. X.-L. Qi, T.L. Hughes, S.-C. Zhang, Phys. Rev. B **82**, 184516 (2010)
19. S.B. Chung, X.-L. Qi, J. Maciejko et al., Phys. Rev. B **83**, 100512 (2011)
20. J. Wang, Q. Zhou, B. Lian et al., Phys. Rev. B **92**, 064520 (2015)
21. B. Lian, J. Wang, S.-C. Zhang, Phys. Rev. B **93**, 161401 (2016)
22. V. Kaladzhyan, J. Despres, I. Mandal et al., Eur. Phys. J. B **90**, 211 (2017)
23. J. Wang, B. Lian, S.-C. Zhang, Phys. Rev. B **89**, 085106 (2014)
24. J. Osca, L. Serra, Phys. Rev. B **91**, 235417 (2015)
25. J. Osca, L. Serra, Eur. Phys. J. B **90**, 28 (2017)
26. J. Osca, L. Serra, Phys. Status Solidi B **254**, 1700135 (2017)
27. L. Serra, Phys. Rev. B **87**, 075440 (2013)